THESIS FOR THE DEGREE OF LICENTIATE OF ENGINEERING

Concentration measurements in single particle microscopy

Magnus Röding

Department of Mathematical Sciences
Division of Mathematical Statistics
Chalmers University of Technology and University of Gothenburg
Göteborg, Sweden 2011

Concentration measurements in single particle microscopy
Magnus Röding
NO 2011:7
ISSN 1652-9715

Department of Mathematical Sciences
Division of Mathematical Statistics
Chalmers University of Technology and University of Gothenburg
SE-412 96 Göteborg
Sweden
Telephone +46 (0)31 772 1000

Typeset with LaTeX.
Printed in Göteborg, Sweden 2011

Concentration measurements in single particle microscopy

Magnus Röding

Department of Mathematical Sciences
Division of Mathematical Statistics
Chalmers University of Technology and University of Gothenburg

Abstract

The topic of this thesis is the introduction of two novel methods for using single particle microscopy as a tool for absolute number concentration measurements of Brownian particles. The key idea of both methods is that in order to estimate number concentration, the size of the (three-dimensional) particle detection region has to be estimated. Typically, this size has until now been estimated by means of a separate *a priori* calibration measurement. Thus, in many cases the influence of for example particle brightness and image analysis settings on the final result have been ignored.

In the first paper, we use single particle tracking to estimate the size of the detection region. This is based on modeling the distribution of trajectory lengths within the detection region. The modeling is simplified by assuming that particles enter and exit the detection region only by means of axial diffusion, i.e. parallel to the optical axis and orthogonal to the focal plane.

In the second paper, we study a time series of particle counts known as a Smoluchowski process. We approximate this non-Markov process by a Markov chain and demonstrate that this model can be used to estimate the size of the detection region. This implies that individual particles need not be tracked. We also introduce a method for automatic selection of a threshold for minimum contrast between particles and the image background, based on analyzing the correlations between particle counts in consecutive frames.

In both cases, we perform experimental validation by estimation of the number concentration of different dilutions of a nanosphere water dispersion, and we find close agreement with validation measurements.

Keywords: diffusion, fluorescence microscopy, nanoparticle characterization, number concentration, optical wide-field microscopy, single particle tracking, Smoluchowski process

Acknowledgements

I would like to thank my advisors Mats Rudemo and Aila Särkkä for their support during this work.

I would also like to thank my co-authors Kevin Braeckmans and Hendrik Deschout of the University of Ghent for a rewarding collaboration.

Comments from and discussions with several members of the SuMo Biomaterials center, including but not limited to Jenny Jonasson, Niklas Lorén, Magnus Nydén, and Joel Hagman, have also been important to my progress.

I also extend my thanks to current and former colleagues at the Department of Mathematical Sciences for a fruitful working environment.

List of Papers

The licentiate thesis includes the following papers.

I. **Röding M.**, Deschout, H., Braeckmans K., and Rudemo, M. (2011). Measuring absolute number concentrations of nanoparticles using single particle tracking. *Submitted.*

II. **Röding M.**, Deschout, H., Braeckmans K., and Rudemo, M. (2011). Measuring absolute nanoparticle number concentrations from the Smoluchowski process. *Working paper.*

Contents

Chapter 1

Introduction

The topic of this thesis is absolute particle number concentration measurements using single particle techniques. We are concerned with Brownian particles only, and further we are not concerned with particle identification, tracking or any aspects of experimental methodology *per se*. Nevertheless, we shall begin with an introduction to single particle techniques, competing methods, image processing and analysis, and give an overview of analysis of data from single particle experiments. A detailed discussion of the particulars of this thesis work will follow in the subsequent chapters.

1.1 Introduction to single particle techniques

Single particle and single particle tracking (SPT) techniques have become essential tools in biophysics, nanophysics, biochemistry, and in a plethora of related fields. Whereas traditional ensemble averaging methods experience limitations regarding the spatial resolution, studying individual particles or particle trajectories has the advantage of providing crucial information about phenomena occurring at, in principle, arbitrarily small spatial and temporal scales (Levi and Gratton, 2010). Several scientific advances such as highly sensitive camera sensors, high-quality optics and lasers, improved fluorescence labeling of particles, and increased computer power for image analysis have enabled the emergence of these techniques as routine tools. One of the consequences of this development is that while before, using ensemble-averaging methods, one would estimate average characteristics of particulate matter such as the av-

erage diffusion coefficient, the average size, and so on, nowadays one can use single particle techniques to learn about *distributions* of such characteristics. Interesting and crucial questions such as whether there are rare events or small subpopulations lost in the averaging process can be answered (Saxton, 2009). In fact, even in populations of chemically homogenous macromolecules, there can occur intramolecular variations concerning other properties that can now be resolved (Kelley et al., 2001). Another advantage is that synchronization of large numbers of molecules at a certain reaction stage in a process is no longer necessary if individual molecules can be studied separately (Zlatanova and van Holde, 2006).

Gaining insight into dynamics of single particles or even single molecules has a substantial impact on many scientific fields. Since the advent of SPT techniques in the biosciences during the 1980s and 1990s, see for example Geerts et al. (1988),Gelles et al. (1988),Lee et al. (1991), and Geerts et al. (1991), the interest for the subject has exploded. Perhaps cell biology and biochemistry are the fields which have been revolutionized the most. These areas concern very small spatial and temporal scales, and the cell is a highly inhomogeneous and dynamic environment in which diffusing, mobile macromolecules and more high-level molecular structures interact in a complex manner. Here, SPT has been used to follow the motion of lipid molecules, membrane proteins, and many other types of macromolecules *in situ* (Levi and Gratton, 2007). Also binding kinetics, such as association and dissociation rates, have been estimated to gain understanding of biological pathways in the cell (Mashanov et al., 2006).

1.2 Alternative techniques

Apart from single particle techniques, many other methods can be used to study the diffusive motion of particles, most notably fluorescence recovery after photobleaching (FRAP) and fluorescence correlation spectroscopy (FCS), both being ensemble-average methods. FRAP can be used to measure the diffusion of fluorescent molecules in a small, micrometer-sized area, the key idea being to study the temporal and spatial structure of the fluorescence intensity as the bleached particles gradually spread from the laser-bleached region (Peters et al., 1974; Axelrod et al., 1976). A diffusion coefficient and the fraction of (im)mobile particles can be estimated using a variety of FRAP models (Braeckmans et al., 2003, 2005). There are many applications of FRAP in pharmaceutical research and cell biology (Meyvis et al., 1999; Remaut et al., 2007). The idea of FCS is to study the temporal fluctuations in fluorescence intensities in a small volume. A diffusion coefficient estimate can be acquired from the temporal correlation function (Magde et al., 1972; Gösch and Rigler, 2005). For

example, FCS has been applied to the study of association and dissociation of macromolecular drug complexes and the stability of DNA molecules (de Smedt et al., 2005; Remaut et al., 2007). In this context, dynamic light scattering (DLS) deserves to be mentioned. DLS is based on measuring the scattered light intensity from diffusing particles, and can be used to estimate size distributions and relative concentrations (Vysotskii et al., 2009). DLS is one of the most widely used techniques to estimate size distributions in simple fluids. However, in more complex biological fluids the presence of other scatterers contaminates the measurements substantially (Braeckmans et al., 2010a).

1.3 Experimental setup

A typical single particle microscope setup is a widefield or confocal fluorescence microscope. The sample is preferably illuminated by laser light, since control over the emission wavelength allows for efficient excitation of the fluorescent labels. The images are captured either by illuminating the whole sample at once, collecting photons by a CCD camera (widefield), or by focusing the illumination into a moving diffraction-limited spot, collecting photons locally (confocal laser scanning) (Braeckmans et al., 2010b; Levi and Gratton, 2010; Zlatanova and van Holde, 2006). Typically, stable, fluorescently labeled, manmade macromolecules, like for example polystyrene nanospheres, are used as tracer particles (Braeckmans et al., 2010a; Deniz et al., 2008). Another option is fluorescent semiconductor nanocrystals (quantum dots), which can provide for dramatically increased contrast and decreased background illumination but on the other hand suffer from blinking effects (Lim et al., 2003; Frangioni, 2006). It is also possible to attach a single fluorescent dye molecule to a specific location in a biological macromolecule, or to attach fluorescent protein probes to any other protein by using recombinant DNA technology (Zlatanova and van Holde, 2006).

1.4 Particle detection and tracking

Prior to any particle detection, some basic image analysis steps are usually performed, like unsharp filtering, background subtraction, and so on (Braeckmans et al., 2010b). Provided that particles are sufficiently far apart (measured in the focal plane) so that the distance between them exceeds the diffraction limit, each individual particle will typically be seen as a Gaussian or Gaussian-like intensity distribution in the image as long as the particle is in focus. The po-

sition along the focal plane of the particle can be estimated by computing the center of this intensity distribution according to some model, given that a small set of pixels have already been identified as a 'candidate particle', typically by a thresholding operation or by direct search for a local intensity maxima. This can involve computing the centroid (the intensity weighted mean position) of the particle, fitting a two-dimensional Gaussian bell curve using for example least squares, or estimating the cross-correlation between the image and some kernel function (Cheezum et al., 2001; Carter et al., 2005). Note that it is not uncommon that the particle size in single particle experiments is so small (less than ∼200 nm) so that it is impossible to optically resolve it in the visible light spectrum according to Abbe's law (Walter et al., 2008). However, it is not the particle *per se* that is imaged in fluorescence microscopy, but the intensity distribution of its photon emission. Additionally, this distribution is convolved with a Gaussian point spread function with a Full Width at Half Maximum depending on the emission wavelength and the numerical aperture (Holtzer and Schmidt, 2010) (more precisely, the point spread function is an Airy disk closely resembling a Gaussian (Saxton and Jacobson, 1997)).

The localization accuracy in particle detection has been subject to substantial interest. Even though the detailed structure of a diffraction limited spot are not observable, the accuracy with which the center of the spot can be estimated is typically far better than the diffraction limit would suggest. Depending on the image background, illumination, fluorescence intensity, signal-to-noise and/or signal-to-background ratios, particle size, optical resolution and magnification, pixel size, CCD sensor noise, finite camera integration times, and image analysis methods, the accuracy and precision can vary. For example, Yildiz et al. (2003) and Yildiz and Selvin (2004) report a localization uncertainty of about 1.5 nm for fitting of a Gaussian point spread function, whereas Levi et al. (2006) reported that a 'pattern recognition' approach yielded a localization uncertainty of about 2 nm without any parametric assumptions on the distributional shape, and Bausch and Weitz (2002) reported an uncertainty of about 5 nm for quantum dot tracking. Notably, as long as only the center of the spot is estimated, tracking can only be performed in two dimensions.

Several authors have presented theoretical results for the localization error. Thompson et al. (2002) assumed a Gaussian least-squares fitting procedure and came to the conclusion that the variance of the center estimate in each direction is $(s^2 + a^2/12)/N + (8\pi s^4 b^2)/(a^2 N^2)$, where s is the standard deviation of the point spread function, a is the physical pixel size, N is the number of collected photons, and b is the standard deviation of the background noise. Ober et al. (2004) assumes a maximum likelihood fitting procedure and computed the Fisher information matrix to show that the lower bound on the localization error is $\lambda_{\mathrm{em}}/(2\pi n_{\mathrm{a}}\sqrt{\gamma A t})$, where λ_{em} is the emission wavelength, n_{a} is the

numerical aperture, γ is the efficiency of the optical system (i.e. the probability that a photon emitted from a fluorescent particle is detected), A is the photon emission rate of the particle, and t is the acquisition time. However, these approaches do not take into account the fact that particles are typically in motion so that a longer acquisition time does not only impose a larger number of collected photons but also a distorted, non-radial spot. The problem of assessing localization error for particles in motion is recognized by Savin and Doyle (2005), who distinguish between 'static' and 'dynamic' errors, and by Destainville and Salomé (2006), who introduces corrections for diffusion coefficient estimation under localization error. It seems that the most complete account to this date is Mortensen et al. (2010), who investigate a number of fitting procedures and point out some over-optimistic results previously reported, and also cover the case of a non-radial intensity profile. Although localization error depends on the settings of the experiment and postprocessing and is not always a critical issue, it has been reported that localization uncertainty can affect both the qualitative and quantitative interpretation of particle trajectories, for example that Brownian motion can mistakenly be interpreted as anomalous (sub)diffusion (Martin et al., 2002).

Once candidate particle spots have been identified in all images of a sequence, the spots can be connected to form tracks using a multitude of methods. The theoretically most appealing method would be the so called multiple hypothesis testing scheme first described by Reid (1979), where a set of data association hypotheses are generated to account for all possible associations of tracking (or a suitable subset of those), identifying the most likely hypothesis according to some criterion. However this approach is computationally heavy since the state space dimension explodes very quickly. The aim of most approaches is to approximate this method in some way, and taking into account the fact that the trajectories can cross each other, particles can move in and out of the frame, in and out of the depth of field, merge either by fusion or occlusion to form a single particle, split into two or more particles, temporarily disappear due to misdetection and so on. For example, one of the most commonly used methods among experimental practitioners is the nearest neighbor algorithm, which is based on finding particle positions close to each other in consecutive frames (Apgar et al., 2000; Crocker and Grier, 1996). This is a valid principle as long as individual particles are far apart and the amount of noise and clutter is sufficiently low. Alternatively, one can formulate a linear optimization problem by assigning a cost to each track assignment in a first greedy step between consecutive frames and a second temporally global step (Jaqaman et al., 2008). Notably, some more recent approaches formulate both particle detection and tracking as one single problem, making use of prior knowledge from previous frames to assist particle detection in the current frame (Smal et al., 2008). It is not uncommon to reduce the influence of noise by excluding short tracks in

any further analysis, see Braeckmans et al. (2010a) and Jaqaman et al. (2008).

1.5 Diffusion coefficient estimation

Often diffusing particles are Brownian with independent Gaussian increments. We consider the estimation of a diffusion coefficient from a set of Brownian particles. Consider a monodisperse ensemble with some (common) diffusion coefficient D, with negligible particle-particle interaction on account of a sufficiently low concentration. The Brownian motion $X(t)$, $t \geq 0$, is characterized by the so called mean squared deviation (MSD) property

$$\mathrm{E}[\|X(t) - X(0)\|^2] = 2\mathcal{N}Dt, \tag{1.1}$$

where $\mathcal{N}$ is the number of dimensions (Berg, 1993). Typically, particles diffuse in $\mathcal{N} = 3$ dimensions but their motion can only be observed in $\mathcal{N} = 2$ dimensions. Particle trajectories are not observed continuously, but in a series of (typically equidistant) time points corresponding to the frames in a video. On account of a finite detection region size, an individual particle is only observed in a finite number of frames K, the track length. The observed trajectory is then $r_1, r_2, ..., r_K$ ($\mathcal{N}$-dimensional vectors, K random). Each position along the trajectory can be written as the previous position plus a Gaussian increment,

$$r_i = r_{i-1} + \Delta G_i, \tag{1.2}$$

where ΔG_i, $i = 1, ..., K-1$, is an $\mathcal{N}$-dimensional vector of normally distributed independent components, each with mean zero and variance $2D\Delta t$. The traditional approach to estimate diffusion coefficients in the single particle tracking literature is to compute an empirical value of the MSD for different time lags and averaged over a set of particle tracks, which for Brownian motion asymptotically yields a straight line, and estimate the slope of this line to extract an estimate of the diffusion coefficient (Saxton, 1997). However, here we consider maximum likelihood estimation instead. Suppose we observe J tracks, the j:th track having length $K = k_j$. The maximum likelihood estimator for the diffusion coefficient D based on the j:th track is

$$\hat{D}_j = \frac{\sum_{i=1}^{k_j-1} \|\Delta G_i\|^2}{4(k_j - 1)\Delta t}, \tag{1.3}$$

where Δt is the time lapse between consecutive frames. It can be shown that $\hat{D}_j$ follows the gamma distribution,

$$\hat{D}_j \sim \Gamma\left(k_j - 1, \frac{D}{k_j - 1}\right), \tag{1.4}$$

with the density function

$$f_\gamma\left(x; k_j - 1, \frac{D}{k_j - 1}\right) = \frac{x^{k_j-2} e^{-\frac{(k_j-1)x}{D}}}{\left(\frac{D}{k_j-1}\right)^{k_j-1} (k_j - 2)!}. \tag{1.5}$$

Based on all observed tracks, under assumed independence, the log-likelihood for D becomes

$$l(D) = \sum_j \log f_\gamma\left(x; k_j - 1, \frac{D}{k_j - 1}\right), \tag{1.6}$$

yielding the maximum likelihood estimator

$$\hat{D} = \frac{\sum_j (k_j - 1)\hat{D}_j}{\sum_j (k_j - 1)}. \tag{1.7}$$

Exact confidence intervals for D can be attained. See also Saxton (1997) who studies the distribution of estimated diffusion coefficients by simulation.

There are however two problems with this simple approach. First, exact confidence intervals for D are conditional on the track lengths $k_1, k_2, ..., k_J$, which are observations from the distribution $P(K = k|D)$. In an SPT experiment, the parameters of the data acquisition like time lapse, video length and so on are naturally non-random, consequently the number of observed tracks will be random. Second, no account is taken of localization error. The latter has been recognized at least as far back as Qian et al. (1991).

Kvarnström (1991) developed a model assuming that the observed motion was a Brownian motion with diffusion coefficient σ, with each particle position being distorted by a normally distributed error with standard deviation σ_e. By assuming that the particles consist of two populations, mobile and immobile, the diffusion coefficient, the error, and the population proportions could be consistently estimated using the Expectation Maximization (EM) algorithm. It seems unlikely however that the 'dynamic' localization error, caused by motion blur, can be represented by a (radially symmetric) normal distribution. This is confirmed by Savin and Doyle (2005) who demonstrated that static localization noise and motion blur affect an MSD plot in qualitatively different ways. Montiel et al. (2006) analyzed the properties of the maximum likelihood estimator of the diffusion coefficient given that normal localization noise is present but unaccounted for.

1.6 Trajectory analysis

Apart from estimating diffusion coefficients, there is a wide range of characteristics of single particle trajectories that can be analyzed. We will briefly cover the literature on this topic.

Analysis of size distributions is an important application of SPT. Size distributions are intimately related to distribution of diffusion coefficients by the Stokes-Einstein relation. As Finder et al. (2004) conclude, Dynamics Light Scattering is a fast and convenient method for size distributions, but often fails with complex, multi-modal distributions, and can be heavily biased toward larger particles which scatter more light. Since SPT requires no special sample preparations and gives results consistent with manufacturer results, they find SPT a functional method for estimating size distributions in the sub-micron range. Braeckmans et al. (2010a) use a maximum entropy framework to estimate size distributions taking the statistical uncertainty of diffusion coefficient estimation into account. They demonstrate the usefulness of SPT sizing in undiluted biological fluids like blood. None of these address the issue of absolute concentrations, however. Du et al. (2010) on the other hand suggests that SPT can be used for measuring absolute number concentrations using NanoSight equipment (Malloy and Carr, 2006), but required a pre-calibration using a reference sample.

Valentine et al. (2001) did localized measurements of mechanical microenvironments of inhomogeneous soft materials, using particles smaller than the characteristic length scale of the material structure and identifying different local diffusion coefficients. Crocker et al. (2000) did microrheological measurements in soft viscoelastic media (that both store and dissipate energy when subjected to external stress), and was able to determine the local shear modulus from the diffusive motion of tracer particles by interpreting the thermal motion of the medium as a fluctuating strain field which can be observed through the Brownian motion of the tracer particle. Apgar et al. (2000) did measurements of heterogeneities in solutions of actin, which forms the building blocks of the cytoskeleton. It should be mentioned that the study of heterogeneity of solutions and material using single particle tracking methodology has almost exclusively been performed by studying empirical and theoretical MSD curves. This makes it difficult to differentiate between heterogeneities in the form of a temporally and spatially variable diffusion coefficient and anomalous sub(diffusion) which can emerge in the cell, supposedly as a consequence of viscoelasticity in the cytoplasm and nucleoplasm induced by molecular crowding (Guigas and Weiss, 2008). To the author's knowledge, no attempt has been made to model a variable diffusion coefficient globally in space and/or time. The focus has rather

been on trying to classify each trajectory individually as belonging to one of two or more populations, i.e. small or large diffusion coefficient, normal or anomalous diffusion, and so on. It is noteworthy that there exists a rich literature on the topic of diffusion coefficient and drift estimation in heterogeneous systems in mathematical finance and econometrics, where diffusions of the form

$$dX_t = b(X_t; \theta)dt + \sigma(X_t; \theta)dB_t \tag{1.8}$$

occur regularly, and estimation schemes for discrete observations from such processes exist (Sørensen, 2009), but that these methods seem not to have reached the single particle tracking community.

There are also more general attempts to identify different modes of motion in single particle trajectories. For example, Ghosh and Wirth (2007) studies diffusing receptors at the cell surface and differentiates directed motion from pure Brownian diffusion by using temporal correlations in the movement of the particle. Helmuth et al. (2007) uses a supervised learning approach with a support vector machine to identify confined motion, diffusion, and directed motion from experimental data of viruses in host cells. The pattern recognition uses different features extracted from the experimental tracks, see Rudnick and Gaspari (1987) and Coscoy et al. (2007). Wieser et al. (2008) base their work on computing test statistics to compare cumulative distributions of experimentally observed increments with simulated increments for different modes of motion.

Chapter 2

Introduction to papers

The topic of the two papers that constitute this thesis is *absolute (nano)particle number concentration measurements*. The term *number* concentration emphasizes the fact the it is the particle count and not the mass or volume concentration that can be estimated by studying particle motion, as additional information on particle mass and/or volume would otherwise have to be accessible. The experimental setting is essentially the same for both papers. Assume that we observe a set of Brownian particles, diffusing freely in a liquid suspension, typically water or possibly some more complex biological fluid like blood. Further, assume that the concentration of particles is sufficiently low, in order to assure that particle-particle interaction is negligible. In the physics literature, a Brownian motion $X(t)$ with $t \geq 0$ and $X(t)$ in $\mathbf{R}^{\mathcal{N}}$ with some diffusion coefficient D is typically characterized by the so called *mean squared deviation* property Berg (1993),

$$\mathrm{E}[\|X(t) - X(0)\|^2] = 2\mathcal{N}Dt, \tag{2.1}$$

which describes the evolution of diffusive motion in $\mathcal{N}$ dimensions, where $\mathcal{N} = 3$ for particles moving in space, although we typically observe data only for $\mathcal{N} = 2$. In the mathematics literature, the definition is usually more explicit and restrictive, defining Brownian motion in terms of independent Gaussian increments, although this is the usual assumption in most physics works as well.

Assume that in the (approximate) center of the liquid suspension, there is a detection region inside of which particles can be detected (and possibly tracked) and outside of which they cannot be detected. More specifically, we assume that no walls of the liquid suspension are close to the detection volume which

could otherwise compromise the assumption of free diffusive motion. We model the detection region as a rectangular box, see Fig. 2.1. The lateral dimensions are determined by the microscope field of view. Note that the field of view (i.e. the lateral dimensions of the detection region) can be calibrated separately (e.g. through a calibration grid). The axial dimension, which we will refer to as the tracking depth, will be estimated using different statistical models. We assume that one or several time-lapse video sequences with sampling interval Δt (between consecutive frames) is acquired and that particle positions are estimated from these video sequences. We demonstrate two different approaches to con-

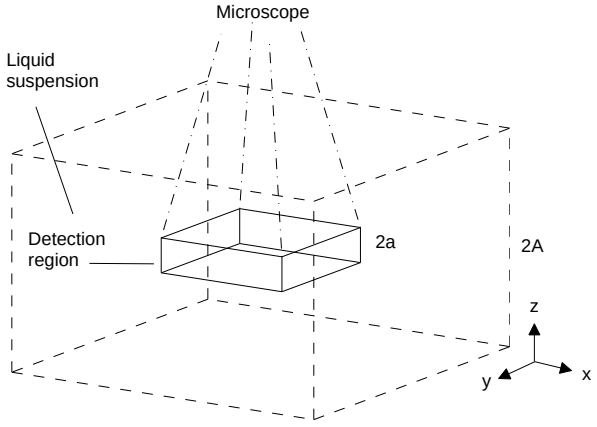

Figure 2.1: An illustration of the experimental setup. The detection region is modeled as a rectangular box centered in the liquid suspension. Particles outside the detection region cannot be observed. The tracking depth is $2a$, and the thickness of the liquid suspension is $2A$.

centration measurements using single particle techniques. In Paper I, we use single particle tracking (SPT) and develop a model for the distribution of track (trajectory) lengths based on diffusion coefficient, tracking depth, sampling intervals and other parameters. This leads to quite accurate estimation of the tracking depth, and consequently the particle number concentration can easily be obtained. In Paper II, no actual tracking of the particles is performed. Rather, the number of detected particles in each individual frame forms the basis of a time series analysis of the so called Smoluchowski process, named af-

ter famous Polish physicist M. von Smoluchowski. We demonstrate that these quite different methods both lead to concentration measurements which are in good correspondence with reference values and that the results are remarkably similar. We proceed with a detailed discussion of some selected parts of the ideas of the two papers as a complement to the descriptions contained within Papers I and II.

2.1 Paper I

2.1.1 Model

Assume that a particle is observed at K equidistant time points (observed in K consecutive frames of a time-lapse video sequence). After these K observation, the particle exits the detection region. The same physical particle may very well enter the detection region again, but will then give rise to more than one track. The K positions, denoted by $r_1, r_2, ..., r_K$, can be written as the previous position plus a (independent) Gaussian increment, i.e. $r_i = r_{i-1} + \Delta G$, where ΔG is an $\mathcal{N}$-dimensional vector of normally distributed independent components, each with mean zero and variance $2D\Delta t$. We refer to K as the track length. Our main concern is to develop a model for the track length distribution, which depends primarily on the size of the detection region and the diffusion coefficient. The smaller the detection region, the shorter the tracks are on average. The smaller the diffusion coefficient, the longer the tracks are on average. See Fig. 2.2 for an illustration of tracking of diffusing polystyrene nanospheres in water solution. Since the lateral dimensions of the detection region are typically much larger than the axial dimension (for the experimental data analyzed herein, a factor of about 50), the major reason why particles enter and exit the detection region is that of (axial) diffusion parallel to the optical axis (the z-direction). Therefore, mostly to reduce the computational burden, we will introduce a simplification by assuming that particles are entering and exiting the detection region *only* by means of axial diffusion. The three-dimensional (3D) system is hence replaced by a one-dimensional (1D) model. The track length distribution is under this approximation a function of the diffusion coefficient, the tracking depth, the sampling interval, and (to a limited extent) the thickness of the liquid suspension, but not of the lateral dimensions of neither the detection region nor the liquid suspension.

Assume that particles diffuse within the suspension $[-A, A]$. They are detected within the detection region $[-a, a]$, and are effectively invisible otherwise. Hence, the thickness of the liquid suspension is $2A$ and the tracking depth

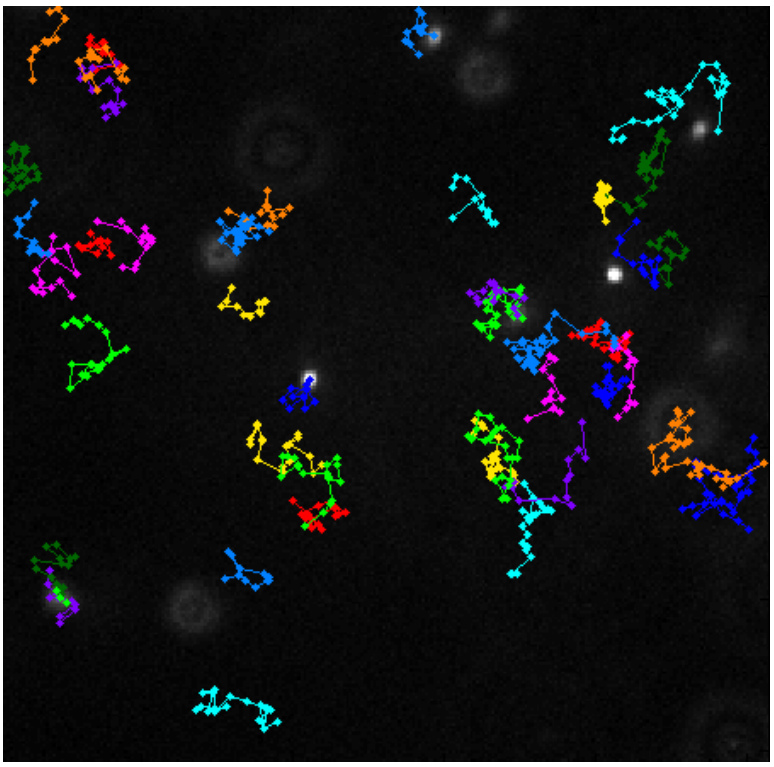

Figure 2.2: Automatically identified trajectories of diffusing polystyrene nanospheres in water solution. Note that the trajectories are unequally (and randomly) long, due to a finite detection region size. Image is acquired using methods described in Braeckmans et al. (2010a).

is $2a$. We employ a 1D Gaussian random walk model with increments of mean zero and variance $2D\Delta t$ to describe the particle motion. Let ϕ denote the standard normal density and Φ the standard normal cumulative distribution function. Assuming diffusion equilibrium, particles are uniformly distributed over $[-A, A]$. Consequently, particles outside of the detection region are uniformly distributed over $[-A, -a] \cup [a, A]$. The probability density of these particles' positions in the following time step is hence a convolution of a uniform density with a Gaussian density (in this context commonly called the *Gaussian propagator*). Restricting to the interval $[-a, a]$ and by normalizing, we obtain the conditional probability density $f(z)$ of the position of a particle that has just

entered the detection region,

$$f(z) = \begin{cases} \frac{h(z)}{\int_{-a}^{a} h(z)dz}, & z \in [-a, a] \\ 0, & z \notin [-a, a] \end{cases} \tag{2.2}$$

where

$$\begin{aligned} h(z) &= \frac{1}{2(A-a)} \left(\Phi\left(\frac{z+A}{\sqrt{2D\Delta t}} \right) - \Phi\left(\frac{z+a}{\sqrt{2D\Delta t}} \right) + \right. \\ &\left. \Phi\left(\frac{z-a}{\sqrt{2D\Delta t}} \right) - \Phi\left(\frac{z-A}{\sqrt{2D\Delta t}} \right) \right). \end{aligned} \tag{2.3}$$

Detailed calculations are available in Appendix A. We want to compute the probability distribution of the track length once a particle enters the detection region. Regard such a particle and let Z_k, $k \geq 1$, denote the particle's kth spatial (axial) position after entering the detection region; thus $-a \leq Z_1 \leq a$ by definition. The track length is the largest integer K such that $-a \leq Z_k \leq a$ for $1 \leq k \leq K$ (the largest number of consecutive frames in which the particle is detected). Consider a particle that resides in the detection region for K consecutive frames. We define f_k as the (non-normalized) probability density of a particle after k steps assuming that $k \leq K$, more precisely

$$f_k(z) = \frac{d}{dz} P(Z_k \leq z \text{ and } K \geq k), \qquad k \geq 1. \tag{2.4}$$

By definition $f_k(z)$ is zero outside of $[-a, a]$. For the first position that the particle is within the detection region, i.e. $k = 1$, the probability density is given by Eq. (2.2) and is illustrated in Fig. 2.3 as f_1. To compute the probability density of the particle in step 2, f_1 is convolved with the Gaussian propagator

$$G(z) = \frac{1}{\sqrt{2D\Delta t}} \phi\left(\frac{z}{\sqrt{2D\Delta t}} \right), \tag{2.5}$$

the result of which is shown in Fig. 2.3 as $f_1 * G$. However, since we have assumed that the particle resides in the detection region for K steps (K now assumed larger than 2), it cannot be outside $[-a, a]$ and the probability density has to be truncated as is illustrated in Fig. 2.3 as f_2. Therefore, more generally, the probability density f_k can be calculated from f_{k-1} according to

$$f_k(z) = \begin{cases} \int_{-\infty}^{\infty} f_{k-1}(z_0) G(z - z_0) dz_0, & z \in [-a, a] \\ 0, & z \notin [-a, a] \end{cases} \tag{2.6}$$

for $k > 1$. Thus we can compute f_k recursively from Eq. (2.6) using $f_1 = f$ with f given by Eq. (2.2). The probability that the particle is within the detection region at time step k is then calculated from

$$P(K \geq k) = \int_{-a}^{a} f_k(z) dz. \tag{2.7}$$

We will numerically compute the track length distribution using an *ad hoc*

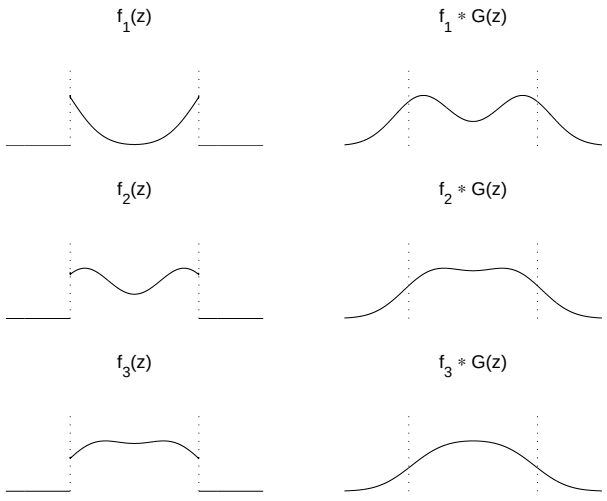

Figure 2.3: Illustration of the procedure for computing the track length distribution. $f_1(z)$ is the probability density of a particle that has just entered the detection region according to Eq. (2.2). Truncation outside of $[-a, a]$ of the convolution $f_1 * G(z)$ yields a non-normalized density $f_2(z)$ which integrates to the probability that the particle still remains in the detection region for a second sampling time point, and so forth.

convolution scheme based on exact interpolation using Gaussian radial basis functions described in detail in Appendix B.

2.1.2 Estimating tracking depth

Suppose that the observed ensemble of particles is monodisperse, i.e. all particles share a common diffusion coefficient, and that this diffusion coefficient is known. We can then construct a maximum likelihood estimate $\hat{a}$ of a by fitting the track length distribution of Eq. (B.12) to an experimentally observed track length distribution. Suppose we have observed tracks each with a length $k \geq k_{\min}$, and let the number of observed tracks of length k be N_k. The

log-likelihood function $l(a) = l(a; A, \Delta t, D, \{N_k\})$ is

$$l(a) = \sum_{k \geq k_{\min}} N_k \log P_a(K = k | K \geq k_{\min}), \tag{2.8}$$

where the dependence on a is stressed and the dependence on other parameters is suppressed. That the diffusion coefficient D is known, at least approximately, is a reasonable assumption since the diffusion coefficient is readily estimated from the particle tracks.

Since the model is misspecified due to the 1D approximation, we will in addition to the random error also get a small bias, which can be approximately corrected for in the following way. Assume that for the true parameter a the estimation procedure above yields the estimate $\hat{a}$. By estimation in a simulated system with true parameter $\hat{a}$, we get a second estimate $\hat{a}'$. Since a and $\hat{a}$ will be reasonably close, we can assume that the bias at a and the bias at $\hat{a}$ are approximately equal, hence $\hat{a} - a \approx \hat{a}' - \hat{a}$. This yields a corrected estimate $\tilde{a}$ of a,

$$\tilde{a} = 2\hat{a} - \hat{a}'. \tag{2.9}$$

In conclusion, using the model as proposed in the previous sections, the tracking depth readily follows from the diffusion coefficient of the monodisperse set of particles and their track length distribution. Since both characteristics readily follow from the SPT experiment itself, it is no longer necessary to estimate the size of the detection region by performing separate, independent calibration experiments prior to the SPT experiment. See Fig. 2.4 for a comparison between model and empirical data for the track length distribution.

2.1.3 Estimating number concentration

Let $\bar{N}$ denote the estimated mean number of particles per frame. Assuming that the length unit is μm, an estimate for number concentration is then

$$\hat{c} = \frac{\bar{N}}{8\hat{a}a_x a_y 10^{-12}} \text{ particles/ml}. \tag{2.10}$$

We can compute the estimate $\bar{N}$ from counting the number of tracks in the SPT movie(s). Let n be the total number of frames of the movie(s). Let N_k as earlier be the number of observed tracks of length k. The number of observed particle *positions* is the sum of all the track lengths. Dividing by the number of frames in the movie(s), this number provides an estimate of the mean number of particles per frame. We estimate $\bar{N}$ by

$$\bar{N} = \frac{1}{\hat{p}_{\text{obs}}} \frac{1}{n} \sum_{k \geq k_{\min}} k N_k. \tag{2.11}$$

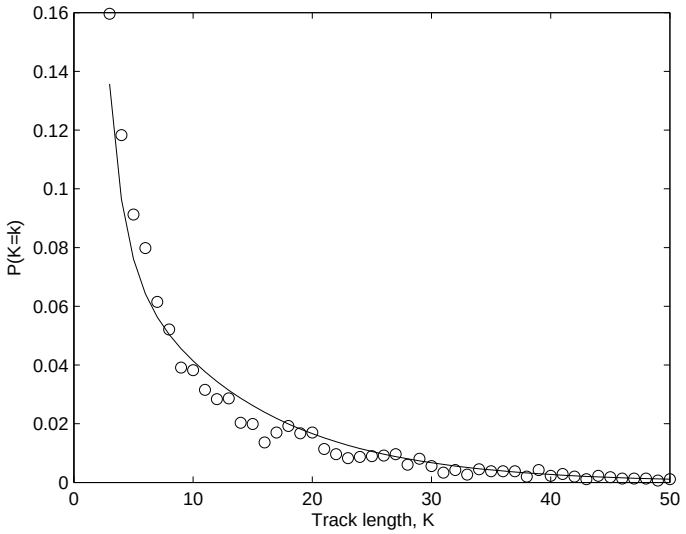

Figure 2.4: An example of an experimentally observed track length distribution and the model fitted by maximum likelihood.

The factor $\hat{p}_{\text{obs}}$ requires a detailed explanation. Recall that it is not uncommon to reduce the influence of noise by excluding short tracks in any SPT analysis, see for example Braeckmans et al. (2010a) and Jaqaman et al. (2008). Suppose we discard tracks of length $k < k_{\min}$. As a consequence, a proportion of the particle positions inside the detection region are not part of an observed track. Not taking these 'unobserved' particle positions into account would cause underestimation of the concentration. Let $\hat{p}_{\text{obs}}$ be the estimated probability of a random particle *position* within the detection region to be observed, i.e. be part of an observed track. We let

$$\hat{p}_{\text{obs}} = \frac{\sum_{k \geq k_{\min}} k P_{\hat{a}}(K = k)}{\sum_{k \geq 1} k P_{\hat{a}}(K = k)}, \tag{2.12}$$

and using this correction factor we can make $\bar{N}$ (approximately) unbiased. The model is experimentally verified by performing SPT experiments, see Paper I page 4 for details. SPT concentration are compared to reference values computed from the particle diameter and the density of the water-particle solution, see Fig. 2.5.

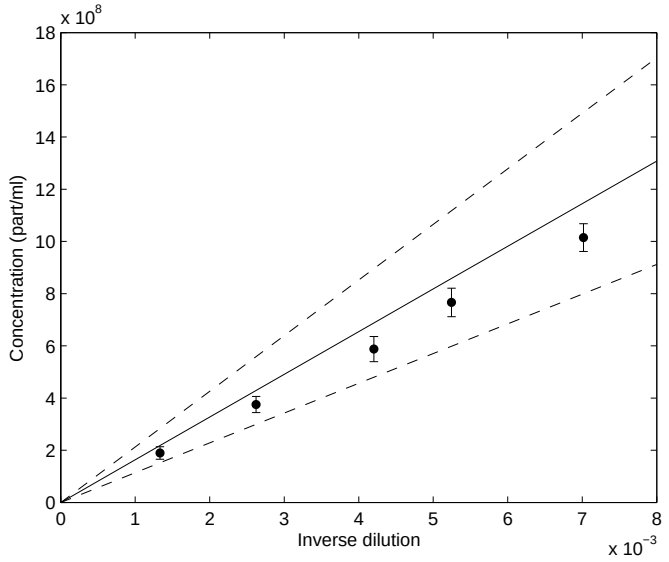

Figure 2.5: Estimated concentrations for five different dilutions with estimated 95 % confidence intervals. The solid and dashed lines show the reference values with estimated 95 % confidence intervals.

2.2 Paper II

2.2.1 Model

In the second paper, we assume that the diffusion coefficient D can be estimated prior to the concentration measurement. Instead of tracking particles, we count the number of particles in each individual frame, and study the resulting stochastic process. This bears some resemblance to both Fluorescence Correlation Spectroscopy (FCS), see Gösch and Rigler (2005), and Particle Image Correlation Spectroscopy (PICS), see Semrau and Schmidt (2007), in which the temporal and/or spatial correlation structure is used to estimate diffusion coefficients. Suppose we acquire M videos and hence collect discrete observations of M independent so called Smoluchowski processes $X^{(m)}(t)$, $m = 1, ..., M$, observed in diffusion equilibrium, observing N_m counts for the m:th video. Denote the n:th observation of the m:th process by $x_n^{(m)}$. Obviously, from one observation to the next, a number of particles has entered and a number of particles has left the detection region. We intend to develop an approximate

Markov chain model for these transitions, in the general case from X_n to X_{n+1}. Assume that

$$X_{n+1} = X_n - O_n + I_n, \tag{2.13}$$

where O_n is the number of particles (out of the X_n particles initially present) exiting the detection region between the observations X_n and X_{n+1}, and I_n is the number of particles entering the detection region between these observations. Without any additional prior knowledge and considering that we are in diffusion equilibrium, a reasonable (but approximate) assumption is that the X_n particles in frame n are uniformly distributed within the detection region. Hence, by independence and conditionally on $X_n = i$, we assume that O_n follows a binomial distribution with index i and some parameter μ, i.e. $O_n|X_n = i \sim \text{Bin}(i, \mu)$. Furthermore, we assume that I_n follows a Poisson distribution with some parameter λ, $I_n \sim \text{Po}(\lambda)$. Under these assumptions, the sequence $\{X_n\}$ can be described by a Markov chain model, for which the transition probabilities $p_{ij} = P(X_{n+1} = j|X_n = i)$ can be shown to be

$$p_{ij}(\lambda, \mu) = e^{-\lambda} \sum_{k=\max(0,j-i)}^{j} \frac{\lambda^k}{k!} \binom{i}{i-j+k} \mu^{i-j+k}(1-\mu)^{j-k} \tag{2.14}$$

for all $i \geq 0$ and $j \geq 0$ (see Paper II page 23 for details). The stationary distribution of this Markov chain is Poisson with parameter λ/μ. Considering a realization $x_1, ..., x_N$ from one video, we get the log-likelihood function

$$l(\lambda, \mu) = l(\lambda, \mu|x_1, ..., x_N) = \log \frac{(\lambda/\mu)^{x_1} e^{-\lambda/\mu}}{x_1!} + \sum_{i,j} N_{ij} \log p_{ij}(\lambda, \mu), \tag{2.15}$$

where N_{ij} is the number of transitions from i to j. Since μ can be interpreted as the probability

$$\begin{aligned} P_{\text{exit}}(a) = 1 - \frac{(2D\Delta t)^{3/2}}{8a_x a_y a} \\ \left(\frac{2a_x}{\sqrt{2D\Delta t}}\left(2\Phi\left(\frac{2a_x}{\sqrt{2D\Delta t}}\right) - 1\right) + 2\phi\left(\frac{2a_x}{\sqrt{2D\Delta t}}\right) - 2\phi(0)\right) \\ \left(\frac{2a_y}{\sqrt{2D\Delta t}}\left(2\Phi\left(\frac{2a_y}{\sqrt{2D\Delta t}}\right) - 1\right) + 2\phi\left(\frac{2a_y}{\sqrt{2D\Delta t}}\right) - 2\phi(0)\right) \\ \left(\frac{2a}{\sqrt{2D\Delta t}}\left(2\Phi\left(\frac{2a}{\sqrt{2D\Delta t}}\right) - 1\right) + 2\phi\left(\frac{2a}{\sqrt{2D\Delta t}}\right) - 2\phi(0)\right). \end{aligned} \tag{2.16}$$

that a uniformly distributed particle exits the detection region (see Paper II page 25 for details), we can find an estimate $\hat{a}$ of a as a mapping $\hat{a} = a(\hat{\mu})$, where $a(\mu)$ is implicitly defined by the relation $P_{\text{exit}}(a) = \mu$. By the invariance

property, $\hat{a}$ is a maximum likelihood estimate (Pawitan, 2001). To estimate the number concentration $c = c(\lambda, \mu)$, we simply divide the mean number of detected particles per frame by the size of the detection region. We obtain

$$\hat{c} = \frac{\hat{\lambda}/\hat{\mu}}{8\hat{a}a_x a_y 10^{-12}} \text{ particles/ml}, \tag{2.17}$$

where the length unit is μm. Once again by the invariance property, $\hat{c} = c(\hat{\lambda}, \hat{\mu})$ is a maximum likelihood estimate.

2.2.2 Minimum contrast threshold selection

Due to limitations in video quality and automated particle detection, we cannot expect to observe Smoluchowski processes without distortion. This is controlled to some extent by the minimum contrast threshold C, defined as the ratio of the mean intensity I of a candidate particle and the local background intensity B,

$$C = \frac{I}{B}. \tag{2.18}$$

A candidate particle is considered a particle if $C \geq C_{\min}$. We assume that there are two sources of distortion, false negatives and false positives. We assume that each particle has, independent of all other particles both in the same frame and other frames, the same probability of being a false negative and misinterpreted as noise. Hence, the number of false negatives in a frame with $X_n = i$ true particles is binomially distributed with index i and parameter ν_{thin}. In addition, we assume that the number of false positives (ghost particles) is independent of the number of true particles in the frame, and independent of the number of ghost particles in other frames. More precisely, the number of false positives is assumed to be Poisson distributed with parameter ν_{ghost}.

We study the (Pearson) correlation coefficient between consecutive observations for the undistorted Smoluchowski process $\{X_n\}$ given by (see paper II page 27 for details),

$$\rho(X_n, X_{n+1}) = \frac{\text{Cov}(X_n, X_{n+1})}{\sqrt{\text{Var}(X_n)\text{Var}(X_{n+1})}} = 1 - \mu. \tag{2.19}$$

We now consider a distorted Smoluchowski process $\{\tilde{X}_n\}$, defined by

$$\tilde{X}_n = X_n - T_n + G_n, \tag{2.20}$$

where T_n is a binomially distributed number of false negatives, $T_n | X_n = i \sim \text{Bin}(i, \nu_{\text{thin}})$, and G_n is a Poisson distributed number of false positives, $G_n \sim$

$\mathrm{Po}(\nu_{\mathrm{ghost}})$. The correlation between consecutive observations is now (see Paper II page 27 for details)

$$\rho(\tilde{X}_n, \tilde{X}_{n+1}) = \frac{(1-\nu_{\mathrm{thin}})^2\left(\frac{\lambda}{\mu}-\lambda\right)}{\frac{\lambda}{\mu}(1-\nu_{\mathrm{thin}})+\nu_{\mathrm{ghost}}}. \tag{2.21}$$

Note that expression (2.21) is monotonically decreasing as a function of both ν_{thin} and ν_{ghost}. Consequently, it attains its maximum when both these parameters are zero. Therefore, we propose to select the minimum contrast threshold such that it maximizes the (sample) correlation. In Fig. 2.6, we see realizations of the same distorted process for different threshold levels. As we see, the process values are monotonically decreasing with increasing threshold. There is

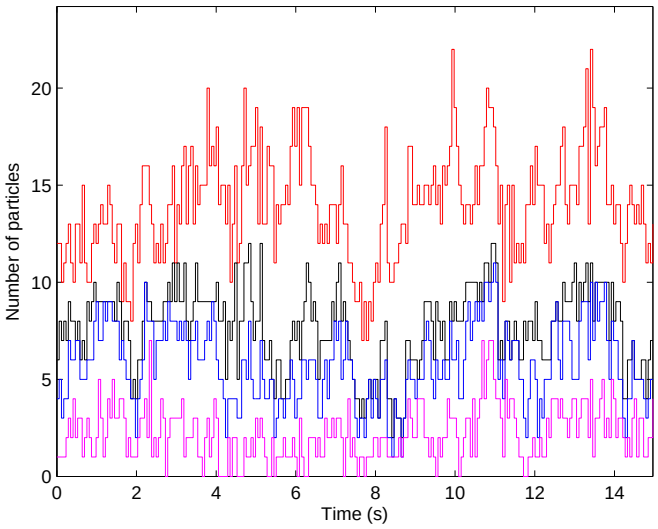

Figure 2.6: Experimentally observed process values for minimum contrast thresholds $C_{\mathrm{min}} = 1.2$ (red), $C_{\mathrm{min}} = 1.4$ (black), $C_{\mathrm{min}} = 1.6$ (blue), and $C_{\mathrm{min}} = 1.8$ (magenta). Naturally, the process values are monotonically decreasing with increasing threshold.

no restriction to the Markov model approximation in this calculation. In fact, we can instead study any physically feasible (we require only finite first and second order moment of the stationary distribution) stationary process $\{W_n\}$ with Pearson correlation between consecutive frames equal to ρ_{true}. This process might be any stationary diffusion process such as anomalous (super- and

sub-)diffusion, directed motion, confined motion, any diffusion of polydisperse particles, and so on. Assume that the mean particle count is θ. Then we obtain the correlation of the distorted process,

$$\rho_{\text{distorted}} = \rho(\tilde{W}_n, \tilde{W}_{n+1}) = \frac{(1-\nu_{\text{thin}})^2\theta}{(1-\nu_{\text{thin}})\theta + \nu_{\text{ghost}}}\rho_{\text{true}}. \tag{2.22}$$

See the Appendix C for further details.

2.2.3 Experimental results

We estimate concentration for the same five data sets as in Paper I. Errors are assessed by bootstrapping (100 replications) and the results are represented as box plots indicating the 2.5%, 25%, 50% (median), 75%, and 97.5% percentiles, see Fig. 2.7. Since the problem of selecting the contrast threshold is not very stable, we also 'pool' all the data together to select a common threshold for all dilutions, see Fig. 2.8. We see now that the concentration estimates are much more consistent with the reference values. In conclusion, the most striking is

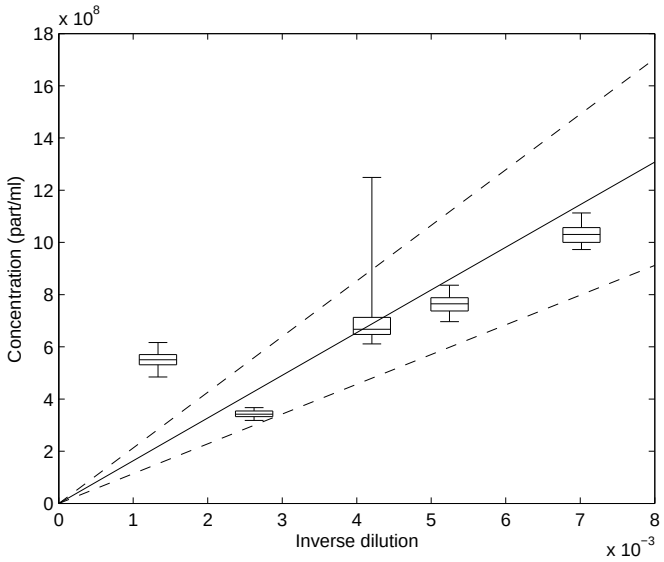

Figure 2.7: Estimated concentrations for five different dilutions, based on 100 bootstrap replications.

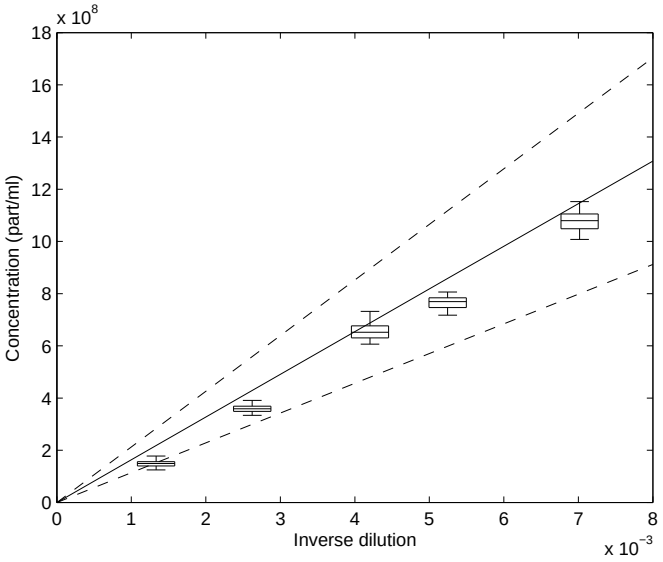

Figure 2.8: Estimated concentrations for five different dilutions, based on 100 bootstrap replications, where a common threshold has been sought for all five dilutions. When 'coupling' the problems like this, the estimates $\hat{c}$ are much more consistent with the reference values.

perhaps the close correspondence between the results of the two very different statistical methods, which is illustrated by overlaying the (point) estimates of both methods in Papers I and II in Fig. 2.9.

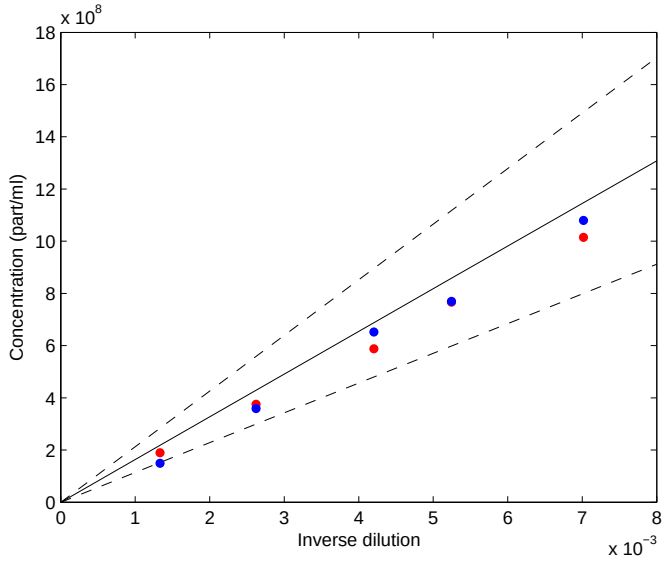

Figure 2.9: Comparison of (point) estimates from both methods, from Paper I (red) and from Paper II (blue).

Chapter 3

Future work

In Paper I, the approximation of the 3D system by a 1D (model) system introduces a bias (even asymptotically). The main reason for this approximation is to speed up the computations. However, simulation studies (not shown) have indicated that a simulation-based inference scheme involving simulated three-dimensional particle systems as a substitute for numerical convolutions can speed up the estimation by at least an order of magnitude, and also remove the asymptotic bias (in fact, using the simulated method of moments, even finite-sample unbiasedness is attainable for the tracking depth, albeit not for the concentration). Another interesting topic is how to optimally select parameters in the particle detection and tracking algorithms. There exist tracking algorithms which incorporate prior knowledge about the observed particle motion. An interesting extension might be to find parameter settings based on goodness of fit test statistics (or arbitrary similarity measures) for the track length distribution. Since in particular the proportion of very short tracks is critically affected by noise, to the extent that these very short tracks are commonly removed in SPT studies, it would be useful to introduce tracking criteria that inherently take these effects into account. Another obvious and currently studied extension is to estimate distribution of absolute concentration for polydisperse (i.e. many diffusion coefficients) particle systems.

In Paper II, the most critical point is the determination of a sensible minimum contrast threshold. The experimental data sets were less well-behaved than the simulated data in this respect. The reason for this is that not all sources of error and noise can be described by the suggested model using Poisson and binomial distributions, and therefore do not conform to the theory in Paper II. This effect is exaggerated by the fact that thresholds for other parameters than

the contrast threshold were set very low for this study, increasing the amount of non-Poissonian noise. It is likely that other data sets acquired with more conservative setting can resolve this issue to some extent. An alternative to the current threshold selection scheme would be to consider some goodness of fit test statistic for comparing the fitted model process to the experimentally observed process. However, initial studies suggest that neither false negatives nor false positives cause a substantial deviation from the model class.

Appendix A

The initial distribution in the detection region (Paper I)

Because of thermal (diffusion) equilibrium, all particles are uniformly distributed over $[-A, A]$ (just consider the asymptotic solution of the diffusion equation with two reflecting boundaries). Consequently, particles outside the detection region are uniformly distributed over $[-A, -a] \cup [a, A]$. This distribution has density function

$$u(z) = \begin{cases} \frac{1}{2(A-a)}, & z \in [-A, -a] \cup [a, A] \\ 0, & \text{otherwise} \end{cases} \tag{A.1}$$

All particles then perform a random diffusive displacement by adding to their position a $N(0, 2D\Delta t)$ increment with density function

$$G(z) = \frac{1}{\sqrt{2D\Delta t}} \phi\left(\frac{z}{\sqrt{2D\Delta t}}\right). \tag{A.2}$$

This density function is simply the Gaussian propagator of free continuous diffusion, the only difference in this case is that it will be applied stepwise in time. The resulting position is the sum of these two stochastic variables, and summation results in convolution of the densities, so that the density of the new position is u convolved with G,

$$h(z) = \int_{-\infty}^{\infty} u(z_0) G(z - z_0) dz_0, \tag{A.3}$$

which becomes

$$h(z) = \frac{1}{2(A-a)\sqrt{2D\Delta t}} \left(\int_{-A}^{-a} + \int_{a}^{A} \right) \phi\left(\frac{z - z_0}{\sqrt{2D\Delta t}} \right) dz_0. \tag{A.4}$$

Simple linear variable substitution yields that

$$\int_{-A}^{-a} \phi\left(\frac{z - z_0}{\sqrt{2D\Delta t}} \right) dz_0 = \sqrt{2D\Delta t} \int_{\frac{z+a}{\sqrt{2D\Delta t}}}^{\frac{z+A}{\sqrt{2D\Delta t}}} \phi(z) dz \tag{A.5}$$

and that

$$\int_{a}^{A} \phi\left(\frac{z - z_0}{\sqrt{2D\Delta t}} \right) dz_0 = \sqrt{2D\Delta t} \int_{\frac{z-A}{\sqrt{2D\Delta t}}}^{\frac{z-a}{\sqrt{2D\Delta t}}} \phi(z) dz, \tag{A.6}$$

which together results in an explicit formula for the convolution,

$$\begin{aligned} h(z) = \\ \frac{1}{2(A-a)} \left(\Phi\left(\frac{z+A}{\sqrt{2D\Delta t}} \right) - \Phi\left(\frac{z+a}{\sqrt{2D\Delta t}} \right) + \right. \\ \left. \Phi\left(\frac{z-a}{\sqrt{2D\Delta t}} \right) - \Phi\left(\frac{z-A}{\sqrt{2D\Delta t}} \right) \right). \end{aligned} \tag{A.7}$$

Appendix B

Numerical convolution scheme (Paper I)

Computing f_k for $k \geq 1$ can not be done analytically, and a fast numerical scheme is proposed. The densities are expanded in a space of n equidistant translates $\{\psi_1, ..., \psi_n\}$ of a Gaussian kernel, where

$$\psi_i(z) = \frac{1}{w}\phi\left(\frac{z - m_i}{w}\right). \tag{B.1}$$

Here, w is the width (standard deviation) of the kernels and m_i is the center of the ith kernel. Further we take $m_i - m_{i-1} = w, i = 2, \ldots, n$, $m_1 = -a$ and $m_n = a$, yielding $w = 2a/(n-1)$. In this way, the probability density is approximated inside $[-a, a]$. More precisely, the approximation of the density f_k is

$$\tilde{f}_k(z) = \sum_j c_j^{(k)} \psi_j(z), \tag{B.2}$$

where the weights $c_j^{(k)}$ are selected by exact interpolation, i.e. by demanding that the approximation be exact at the points $z = m_i$, $i = 1, \ldots, n$. For $k = 1$ we obtain $\tilde{f}_1(m_i) = f_1(m_i)$, $i = 1, \ldots, n$, yielding the linear system

$$U\mathbf{c}^{(1)} = f_1(\mathbf{m}), \tag{B.3}$$

where $\mathbf{c^{(1)}} = (c_1^{(1)}, ..., c_n^{(1)})^T$, $f_1(\mathbf{m}) = (f_1(m_1), ..., f_1(m_n))^T$, and

$$U = \begin{pmatrix} \psi_1(m_1) & \cdots & \psi_n(m_1) \\ \vdots & \ddots & \vdots \\ \psi_1(m_n) & \cdots & \psi_n(m_n) \end{pmatrix}. \tag{B.4}$$

It is guaranteed that Eq. (B.3) has a unique solution $\mathbf{c}^{(1)} = U^{-1} f_1(\mathbf{m})$ since U is invertible (and even positive definite). We refer the reader to Buhmann (2003) for further details on exact interpolation by radial basis functions. In every time step, the diffusive motion of particles is represented by convolving the current particle density with the Gaussian propagator Eq. (2.5). We illustrate the procedure and demonstrate the computation of $\tilde{f}_k$ from $\tilde{f}_{k-1}$. We put

$$f_k^\star(z) = \tilde{f}_{k-1} * G(z) = \int_{-\infty}^{\infty} \tilde{f}_{k-1}(z_0) G(z - z_0) dz_0 \tag{B.5}$$

where we provisionally denote by $f_k^\star(z)$ a (non-truncated) density which is not yet approximated in the Gaussian kernel basis $\{\psi_1, ..., \psi_n\}$. Linearity of convolution yields

$$f_k^\star(z) = \sum_j c_j^{(k-1)} \frac{1}{\sqrt{w^2 + 2D\Delta t}} \phi\left(\frac{z - m_j}{\sqrt{w^2 + 2D\Delta t}}\right), \tag{B.6}$$

and in order to approximate this function within $[-a, a]$, we once again demand that the approximation be exact at the points $z = m_i$, i.e.

$$\sum_j c_j^{(k)} \psi_j(m_i) = \sum_j c_j^{(k-1)} \frac{1}{\sqrt{w^2 + 2D\Delta t}} \phi\left(\frac{m_i - m_j}{\sqrt{w^2 + 2D\Delta t}}\right), \quad i = 1, \ldots, n \tag{B.7}$$

where $\mathbf{c}^{(k)}$ are the weights of the Gaussian kernels at the kth time step. This leads to a linear system with the same matrix U as above. Since the convolution at the points m_i can be written as $V\mathbf{c}^{(k-1)}$, where

$$V = \frac{1}{\sqrt{w^2 + 2D\Delta t}} \begin{pmatrix} \phi(0) & \cdots & \phi\left(\frac{(n-1)w}{\sqrt{w^2+2D\Delta t}}\right) \\ \vdots & \ddots & \vdots \\ \phi\left(\frac{(n-1)w}{\sqrt{w^2+2D\Delta t}}\right) & \cdots & \phi(0) \end{pmatrix}, \tag{B.8}$$

the entire step of convolution and approximation in the Gaussian basis can be written as

$$U\mathbf{c}^{(k)} = V\mathbf{c}^{(k-1)} \tag{B.9}$$

which gives

$$\mathbf{c}^{(k)} = U^{-1} V \mathbf{c}^{(k-1)}. \tag{B.10}$$

The approximation of f_k by $\tilde{f}_k$ can be made arbitrarily accurate by increasing n. For a given n, it is sufficient to compute the matrix $U^{-1}V$ once to describe the diffusive dynamics and hence the change of the weights in every time step. These computations yield the distribution of K. Practically, to compute the cumulative distribution of K we use

$$P(K \leq k) = 1 - \int_{-a}^{a} f_{k+1}(z) dz \approx 1 - \sum_i c_i^{(k+1)}, \tag{B.11}$$

using Eq. (2.7). This yields the distribution

$$P(K = k) = P(K \leq k) - P(K \leq k-1) \approx \sum_i \left(c_i^{(k)} - c_i^{(k+1)} \right), \qquad \text{(B.12)}$$

which is implicitly a function of, most importantly, a and D.

Appendix C

Correlations for a general Smoluchowski process (Paper II)

Consider the perturbed process

$$\tilde{W}_n = W_n - T_n + G_n, \tag{C.1}$$

and we see that

$$\begin{aligned}\mathrm{Cov}(\tilde{W}_n, \tilde{W}_{n+1}) = \mathrm{Cov}(W_n - T_n, W_{n+1} - T_{n+1}) = ... \\ \mathrm{Cov}\left(\sum_{i=1}^{W_n} B_{i,n}, \sum_{j=1}^{W_{n+1}} B_{j,n+1}\right),\end{aligned} \tag{C.2}$$

where $B_{i,n}$ and $B_{j,n+1}$ are all independent and Bernoulli distributed with parameter $1 - \nu_{\mathrm{thin}}$. We get

$$E\left[\sum_{i=1}^{W_n} B_{i,n} \sum_{j=1}^{W_{n+1}} B_{j,n+1}\right] - E\left[\sum_{i=1}^{W_n} B_{i,n}\right] E\left[\sum_{j=1}^{W_{n+1}} B_{j,n+1}\right]. \tag{C.3}$$

Now,

$$E\left[\sum_{i=1}^{W_n} B_{i,n} \sum_{j=1}^{W_{n+1}} B_{j,n+1}\right] = ...$$

$$\sum_{I=0}^{\infty}\sum_{J=0}^{\infty} P(W_n = I, W_{n+1} = J) \times ...$$

$$E\left[\sum_{i=1}^{W_n} B_{i,n} \sum_{j=1}^{W_{n+1}} B_{j,n+1} | W_n = I, W_{n+1} = J\right] = ...$$

$$(1-\nu_{\text{thin}})^2 \sum_{I=0}^{\infty}\sum_{J=0}^{\infty} IJP(W_n = I, W_{n+1} = J) =$$

$$(1-\nu_{\text{thin}})^2 E[W_n W_{n+1}]. \tag{C.4}$$

Similarly,

$$E\left[\sum_{i=1}^{W_n} B_{i,n}\right] = (1-\nu_{\text{thin}})E[W_n], \tag{C.5}$$

and consequently

$$\text{Cov}(\tilde{W}_n, \tilde{W}_{n+1}) = (1-\nu_{\text{thin}})^2 \text{Cov}(W_n, W_{n+1}). \tag{C.6}$$

Since it holds that $\text{Var}(\tilde{W}_n) = (1-\nu_{\text{thin}})\theta + \nu_{\text{ghost}}$, we get that the correlation is

$$\rho_{\text{distorted}} = \rho(\tilde{W}_n, \tilde{W}_{n+1}) = \frac{(1-\nu_{\text{thin}})^2\theta}{(1-\nu_{\text{thin}})\theta + \nu_{\text{ghost}}}\rho_{\text{true}}. \tag{C.7}$$

The calculations are thus valid for any diffusion process under equilibrium. In particular they are valid for the Brownian motion-based Smoluchowski process studied herein, even without the Markov model approximation.

Bibliography

Apgar, J., Tseng, Y., Fedorov, E., Herwig, M., Almo, S., and Wirtz, D. (2000). Multiple-particle tracking measurements of heterogeneities in solutions of actin filaments and actin bundles. *Biophysical Journal*, 79:1095–1106.

Axelrod, D., Koppel, D., Schlessinger, J., Elson, E., and Webb, W. (1976). Mobility measurement by analysis of fluorescence photobleaching recovery kinetics. *Biophysical Journal*, 16:1095–1106.

Bausch, A. and Weitz, D. (2002). Tracking the dynamics of single quantum dots: Beating the optical resolution twice. *Journal of Nanoparticle Research*, 4:477–481.

Berg, H. C. (1993). *Random Walks in Biology*. Princeton University Press.

Braeckmans, K., Buyens, K., Bouquet, W., Vervaet, C., Joye, P., de Vos, F., Plawinski, L., Doeuvre, L., Anglés-Cano, E., Sanders, N., Demeester, J., and de Smedt, S. (2010a). Sizing nanomatter in biological fluids by fluorescence single particle tracking. *Nano Letters*, 10:4435–Ũ4442.

Braeckmans, K., Peeters, L., Sanders, N., de Smedt, S., and Demeester, J. (2005). Three-dimensional fluorescence recovery after photobleaching with the confocal scanning laser microscope. *Biochemica et Biophysica Acta - Biomembranes*, 85:193–207.

Braeckmans, K., Remaut, K., and Vandenbroucke, R. (2003). Line FRAP with the confocal laser scanning microscope for diffusion measurements in small regions of 3-D samples. *Biophysical Journal*, 92:2172–2183.

Braeckmans, K., Vercauteren, D., Demeester, J., and de Smedt, S. (2010b). Single particle tracking. In Diaspro, E., editor, *Nanoscopy multidimensional optical fluorescence microscopy*. Taylor and Francis.

Buhmann, M. D. (2003). *Radial basis functions: theory and implementations*. Cambridge University Press, Cambridge, UK.

Carter, B., Shubeita, G., and Gross, S. (2005). Tracking single particles: a user-friendly quantitative evaluation. *Physical Biology*, 2:60–72.

Cheezum, M., Walker, W., and Guilford, W. (2001). Quantitative comparison of algorithms for tracking single flourescent particles. *Biophysical Journal*, 81:2378–2388.

Coscoy, S., Huguet, E., and Amblard, F. (2007). Statistical analysis of sets of random walks: How to resolve their generating mechanism. *Bulletin of Mathematical Biology*, 2007:2467–2492.

Crocker, J. and Grier, D. (1996). Methods of digital video microscopy for colloidal studies. *Journal of Colloid and Interface Science*, 179:298–310.

Crocker, J., Valentine, M., Weeks, E. R., Gisler, T., Kaplan, P., Yodh, A., and Weitz, D. (2000). Two-point microrheology of inhomogeneous soft materials. *Physical Review Letters*, 85:888–891.

de Smedt, S., Remaut, K., and Lucas, B. (2005). Studying biophysical barriers to DNA delivery by advanced light microscopy. *Advanced Drug Delivery Reviews*, 57:191–210.

Deniz, A., Mukhopadhyay, S., and Lemke, E. (2008). Single-molecule biophysics: at the interface of biology, physics and chemistry. *Journal of the Royal Society Interface*, 5:15–45.

Destainville, N. and Salomé, L. (2006). Quantification and correction of systematic errors due to detector time-averaging in single-molecule tracking experiments. *Biophysical Journal*, 90:L17–L19.

Du, S., Kendall, K., Morris, S., and Sweet, C. (2010). Measuring number-concentrations of nanoparticles and viruses in liquids on-line. *Journal of Chemical Technology and Biotechnology*, 85:1223Ű–1228.

Finder, C., Wohlgemuth, M., and Mayer, C. (2004). Analysis of particle size distribution by particle tracking. *Particles and Particles Systems Characterization*, 22:372–378.

Frangioni, J. (2006). Self-illuminating quantum dots light the way. *Nature Biotechnology*, 24:326–328.

Geerts, H., de Brabander, M., and Nuydens, R. (1991). Nanovid microscopy. *Nature*, 351:765–766.

Geerts, H., de Brabander, M., Nuydens, R., Geuens, S., Moeremans, M., de Mey, J., and Hollenbeck, P. (1988). Nanovid tracking: a new automatic method for the study of mobility in living cells based on colloidal gold and video microscopy. *Biophysical Journal*, 52:775–782.

Gelles, J., Schnapp, B., and Scheetz, M. (1988). Tracking kinesin-driven movements with nanometre-scale precision. *Nature*, 331:450–453.

Ghosh, I. and Wirth, M. (2007). Versatile analysis of single-molecule tracking data by comprehensive testing against monte carlo simulations. *Science Signaling*, 2007:pe28.

Gösch, M. and Rigler, R. (2005). Fluorescence correlation spectroscopy of molecular motions and kinetics. *Advanced Drug Delivery Reviews*, 57:169–190.

Guigas, G. and Weiss, M. (2008). Sampling the cell with anomalous diffusion - the discovery of slowness. *Biophysical Journal*, 94:90–94.

Helmuth, J., Burckhardt, C., Koumoutsakosa, P., Greberb, U., and Sbalzarinia, I. (2007). A novel supervised trajectory segmentation algorithm identifies distinct types of human adenovirus motion in host cells. *Journal of Structural Biology*, 159:347–358.

Holtzer, L. and Schmidt, T. (2010). The tracking of individual molecules in cells and tissues. In Brächle, C., Lamb, D., and Michaelis, J., editors, *Single particle tracking and single molecule energy transfer*. Wiley.

Jaqaman, K., Loerke, D., Mettlen, M., Kuwata, H., Grinstein, S., Schmid, S., and Danuser, G. (2008). Robust single-particle tracking in live-cell time-lapse sequences. *Nature Methods*, 5:695–702.

Kelley, A., Michalet, X., and Weiss, S. (2001). Chemical physics. Single-molecule microscopy comes of age. *Science*, 292:1671–1672.

Kvarnström, M. (1991). Estimation of the diffusion coefficient in a mixture model. *Kwantitatieve Methoden*, 72:1–23.

Lee, G., Ishihara, A., and Jacobson, K. (1991). Direct observation of Brownian motion of lipids in a membrane. *Proceedings of the National Academy of Sciences*, 88:6274–6278.

Levi, V. and Gratton, E. (2007). Exploring dynamics in living cells by tracking single particles. *Cell Biochemistry and Biophysics*, 48:1–15.

Levi, V. and Gratton, E. (2010). Three-dimensional particle tracking in a laser scanning fluorescence microscope. In Brächle, C., Lamb, D., and Michaelis, J., editors, *Single particle tracking and single molecule energy transfer*. Wiley.

Levi, V., Serpinskaya, A., Gratton, E., and Gelfand, V. (2006). Organelle transport along microtubules in xenopus melanophores: Evidence for cooperation between multiple motors. *Biophysical Journal*, 90:318–327.

Lim, Y., Kim, S., Nakayama, A., Stott, N., Bawendi, M., and Frangioni, J. (2003). Selection of quantum dot wavelengths for biomedical assays and imaging. *Molecular Imaging*, 2:50–64.

Magde, D., Elson, E., and Webb, W. W. (1972). Thermodynamics fluctuations in a reactin system: measurement by flouroescence correlation spectroscopy. *Physical Review Letters*, 29:705–708.

Malloy, A. and Carr, B. (2006). Nanoparticle tracking analysis: The Halo system. *Particles and Particles Systems Characterization*, 23:197–204.

Martin, D., Forstner, M., and Käs, J. (2002). Apparent subdiffusion inherent to single particle tracking. *Biophysical Journal*, 83:2109–2117.

Mashanov, G., Nenasheva, T., Peckham, M., and Molloy, J. (2006). Cell biochemistry studied by single-molecule imaging. *Biochemical Society Transactions*, 34:983–988.

Meyvis, T., de Smedt, S., van Oostveldt, P., and Demeester, J. (1999). Fluorescence recovery after photobleaching: A versatile tool for mobility and interaction measurements in pharmaceutical research. *Pharmaceutical Research*, 16:1153–1162.

Montiel, D., Cang, H., and Yang, H. (2006). Quantitative characterization of changes in dynamical behavior for single-particle tracking studies. *Journal of Physical Chemistry B*, 110:19763–19770.

Mortensen, K., Churchman, L., Spudich, J., and Flyvbjerg, H. (2010). Optimized localization analysis for single-molecule tracking and super-resolution microscopy. *Nature Methods*, 7:377–381.

Ober, R., Ram, S., and Ward, E. (2004). Localization accuracy in single-molecule microscopy. *Biophysical Journal*, 86:1185–1200.

Pawitan, Y. (2001). *In All Likelihood: Statistical Modelling and Inference Using Likelihood*. Oxford University Press, Oxford, UK.

Peters, R., Peters, J., Tews, K., and Bahr, W. (1974). Microfluorimetric study of translational diffusion in erythrocyte-membranes. *Biochemica et Biophysica Acta*, 367:282–294.

Qian, H., Sheetz, M., and Elson, E. (1991). Single particle tracking. analysis of diffusion and flow in two-dimensional systems. *Biophysical Journal*, 60:910–921.

Reid, D. (1979). An algorithm for tracking multiple targets. *IEEE Transactions on Automatic Control*, 24:843–854.

Remaut, K., Sanders, N., de Geest, B., Braeckmans, K., Demeester, J., and de Smedt, S. (2007). Nucleic acid delivery: Where material sciences and bio-sciences meet. *Materials Science and Engineering: R*, 58:117Ũ–161.

Rudnick, J. and Gaspari, G. (1987). The shapes of random walks. *Science*, 237:384–389.

Savin, T. and Doyle, P. (2005). Static and dynamic errors in particle tracking microrheology. *Biophysical Journal*, 88:623–638.

Saxton, M. (1997). Single-particle tracking: the distribution of diffusion coefficients. *Biophysical Journal*, 72:1744–1753.

Saxton, M. (2009). Single-particle tracking. In Jue, T., editor, *Fundamental concepts in biophysics*. Springer.

Saxton, M. and Jacobson, K. (1997). Single-particle tracking: Applications to membrane dynamics. *Annual Review of Biophysics and Biomolecular Structure*, 26:373–399.

Semrau, S. and Schmidt, T. (2007). Particle image correlation spectroscopy (PICS): Retrieving nanometer-scale correlations from high-density single-molecule position data. *Biophysical Journal*, 92:613–621.

Smal, I., Draegestein, K., Galjart, N., Niessen, W., and Meijering, E. (2008). Particle filtering for multiple object tracking in dynamic fluorescence microscopy images: Application to microtubule growth analysis. *IEEE Transactions on Medical Imaging*, 27:789–804.

Sørensen, M. (2009). Parametric inference for discretely sampled stochastic differential equations. In Mikosch, T., KreiSS, J.-P., Davis, R., and Andersen, T., editors, *Handbook of Financial Time Series*, pages 531–553. Springer.

Thompson, R., Larson, D., and Webb, W. (2002). Precise nanometer localization analysis for individual fluorescent probes. *Biophysical Journal*, 82:2775–2783.

Valentine, M., Kaplan, P., Thota, D., Crocker, J., Gisler, T., PrudŠhomme, R., Beck, M., and Weitz, D. (2001). Investigating the microenvironments of inhomogeneous soft materials with multiple particle tracking. *Physical Review E*, 64:1–9.

Vysotskii, V., Uryupina, O., Guselńikova, A., and Roldugin, V. (2009). On the feasibility of determining nanoparticle concentration by the dynamic light scattering method. *Colloid Journal*, 71:739–Ũ744.

Walter, N., Huang, C.-Y., Manzo, A., and Sobhy, M. (2008). Do-it-yourself guide: how to use the modern single-molecule toolkit. *Nature Methods*, 5:475–489.

Wieser, S., Axmann, M., and Schütz, G. (2008). Versatile analysis of single-molecule tracking data by comprehensive testing against monte carlo simulations. *Biophysical Journal*, 95:5988–6001.

Yildiz, A., McKinney, J. F. S., Ha, T., Goldman, Y., and Selvin, P. (2003). Myosin V walks hand-over-hand: Single fluorophore imaging with 1.5-nm localization. *Science*, 300:2061–2065.

Yildiz, A. and Selvin, P. (2004). Kinesin walks hand-over-hand. *Science*, 303:676–678.

Zlatanova, J. and van Holde, K. (2006). Single-molecule biology: what is it and how does it work? *Molecular Cell*, 24:317–329.